

PREPARATION OF DIFFERENT SCALE FIBROUS MEMBRANES AND THEIR FILTRATION PROPERTIES

by

Xiao-Xuan MO^{a}, Ni YIN^{a**}, and Fu-Juan LIU^{a,b*}**

^a National Engineering Laboratory for Modern Silk, College of Textile and Clothing Engineering, Soochow University, Suzhou, China

^b Nantong Textile and Silk Industrial Technology Research Institute, China

Original scientific paper
<https://doi.org/10.2298/TSCI200103046M>

In this work, the polyacrylonitrile monolayer/composite nanofibrous membranes were successfully fabricated at different processing parameters. As expected, compared with monolayer membranes, the composite membrane revealed high breaking strength, high breaking elongation, high porosity, and good filtration performance. The composite method used in this article also provides new ideas for designing filter materials.

Key words: electrospinning polyacrylonitrile, filtration performance

Introduction

Air pollution has become a global problem in recent years [1]. Exposure to ambient particulate matter (PM) is associated with a number of adverse health outcomes [2, 3], especially particulates with aerodynamic diameter between PM_{2.5} and PM₁₀ can penetrate into the respiratory system. Air filtration is a low cost way to purify the air. Zhang *et al.* [4] developed high-efficiency polyimide-nanofiber air filters for the high temperature PM_{2.5} removal. Zhang [5] *et al.* found nanocrystals of four unique metal organic framework (MOF) structures were processed into nanofibrous filters (noted as MOFilter) with high MOF loadings in the hazy environment.

Nanofibers are used in a wide range of applications due to their many excellent properties [6]. Due to the larger specific surface area of nanofibers, more contaminants are adsorbed from the surfaces of both air and water, and the useful life of the filter medium is extended [7]. The obtained nanofibers from green electrospinning and ecofriendly thermal cross-linking membranes show not only highly efficient air-filtration performance but also superior photocatalytic and antibacterial activities [8, 9].

Polyacrylonitrile (PAN) nanofibers are good candidates for air filtration media [10, 11] and water purification media. In addition, the researcher engineered three different filter materials that are characterized by the different particles for air filtration [12]. Chen presented a multifunctional filter having PAN nanofibers with embedded commercial P25 and/or TiO₂ bead filler [13].

In this work, the electrospinning technology [14-26] is used to fabricate PAN monolayer/composite nanofibrous membranes. The surface morphology, mechanical properties, porosity, and filtration performance of monolayer/composite membranes were characterized and analyzed systematically. The results showed that composite membranes not only had good mechanical properties, but also excellent porosity and filtration performance. This composite technology provides a novel way for filter materials.

* Corresponding author, e-mail: liufujuan@suda.edu.cn

** Mo, X.-X. and Yin, N. contributed equally

Experimental

The PAN ($MW = 150000$ g/mol) was purchased from Beijing Lark Branch Co. Ltd. and *N, N*-dimethyl formamide (DMF) from Sinopharm Chemical Reagent Co. Ltd.

The PAN powder and DMF solvent were mixed. The mixture was then placed in a thermostatic water bath (60 °C) and stirred at a constant speed for four hours to obtain PAN solutions. In order to prepare the composite membranes, three different concentrations of solutions were electrospun at the same flow rate to fabricate the nanofibrous membrane with different scales.

The surface morphology of the nanofibers was observed by cold field scanning electron microscope (Hitachi S-4800) after gold spraying. The diameters of the fibers were measured by Image J software.

The mechanical properties of the prepared nanofiber membranes were tested by tensile instrument (Instron 5967). The size of the test sample was 10 mm \times 40 mm. The clamping distance was set as 20 mm, and the tensile speed 20 mm per minute.

Porometer 3G was used to determine the pore diameter distribution of the membranes. The samples were cut into the circles with a diameter of 25 mm, and wetted with the profile reagent. The pore size distribution under the humid state and the completely dry state of the sample volatilized by aeration were measured by the instrument.

The filtration performance of the fiber membranes was tested by a filtration performance tester (TSI 8130) to determine the aerosol passage rate of the fiber membrane. The sample was at least 15 cm in diameter and need to be tested five times in different areas.

Results and discussion

Figure 1 exhibits SEM micrographs of the surface of fiber membranes with different flow rates at the solution concentration of 10 %. From fig. 1, the fibers show uniform morphologies at each flow rate, and the diameters of the fibers increase with the increase of the flow rate. The bead structure can be clearly found in the fiber membrane with a flow rate of 1.5 mL/h from the inset in fig. 1(e). This may be that the flow rate is too fast, resulting in a not enough stretching process of the droplets.

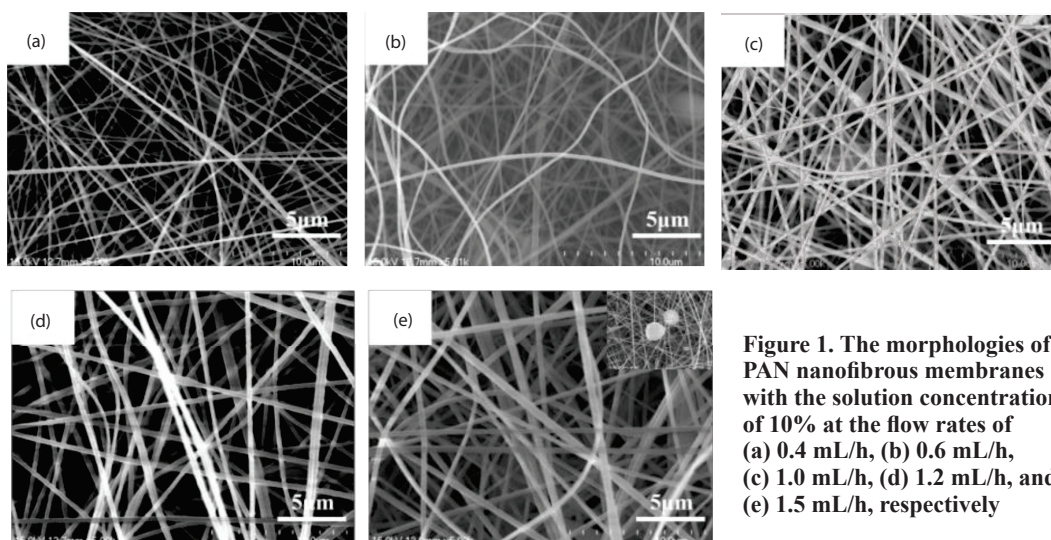


Figure 1. The morphologies of PAN nanofibrous membranes with the solution concentration of 10 % at the flow rates of (a) 0.4 mL/h, (b) 0.6 mL/h, (c) 1.0 mL/h, (d) 1.2 mL/h, and (e) 1.5 mL/h, respectively

In order to further explore the properties of the nanofiber membranes, the appropriate processing parameters of electrospinning were selected. All the solutions were electrospun at the voltage of 18 kV and the collecting distance of 18 cm. When the flow rate is kept at 0.4 mL/h, it can be found that the diameter of nanofiber is much smaller, and its distribution is worse than those of other nanofibers under flow rates of 0.6 mL/h, 1.0 mL/h, and 1.2 mL/h. Moreover, in order to avoid the impact of the bead structure, fig. 1(e), on the performances of the nanofiber membranes, we chose the flow rates of 0.6 mL/h, 1.0 mL/h, and 1.2 mL/h, respectively.

Figures 2 and 3 show the surface morphologies of the fibers at three different flow rates for solution concentrations of 8% and 12%, respectively. It can be obviously seen that the smooth fibers were obtained in all cases. At the same concentration, the larger the flow rate, the larger the nanofibrous diameter.

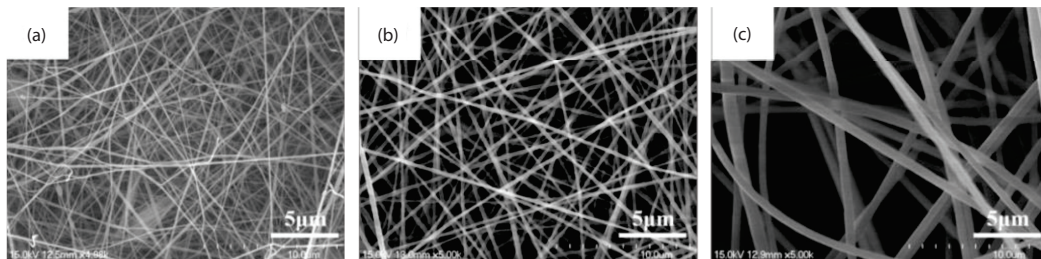


Figure 2. The morphologies of PAN nanofibrous membranes with the solution concentration of 8 % at the flow rates of (a) 0.6 mL/h, (b) 1.0 mL/h, and (c) 1.2 mL/h, respectively

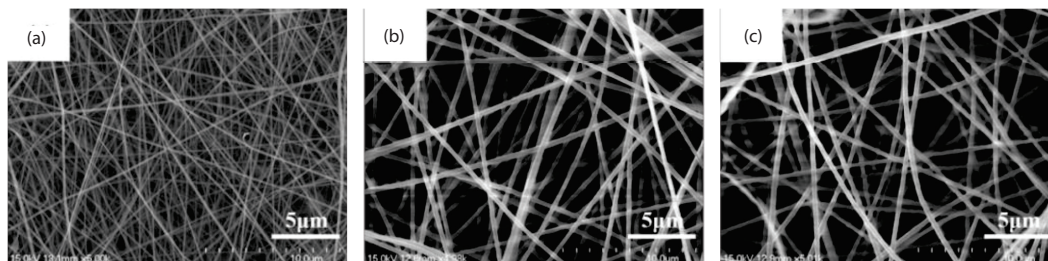


Figure 3. The morphologies of PAN nanofibrous membranes with the solution concentration of 12 % at the flow rates of (a) 0.6 mL/h, (b) 1.0 mL/h, and (c) 1.2 mL/h, respectively

Table 1. The mean diameter and standard deviation of the fibers under different parameters ($n = 100$)

Solution concentrations	Flow rates [mLh ⁻¹]	Average diameter [nm]
8%	0.6	167 ± 27
	1.0	242 ± 23
	1.2	466 ± 39
10%	0.4	187 ± 39
	0.6	259 ± 26
	1.0	295 ± 35
	1.2	483 ± 38
12%	1.5	601 ± 43
	0.6	157 ± 25
	1.0	344 ± 24
	1.2	369 ± 29

The mean diameter and standard deviation of the fibers under different parameters are presented in tab. 1. It is very straightforward to investigate the effect of the solution concentrations and flow rates on the diameter of nanofiber. Based on the standard deviation data, it can be concluded that the larger the flow rate, the more uneven the nanofibers. However, the effect of solution concentration on fiber diameter has no obvious regularity. Hence, in this work, the influence of flow rate on fiber diameter is considered to be more significant than that of solution concentration.

In this work, the mechanical properties of all fiber membranes were tested and analyzed systematically.

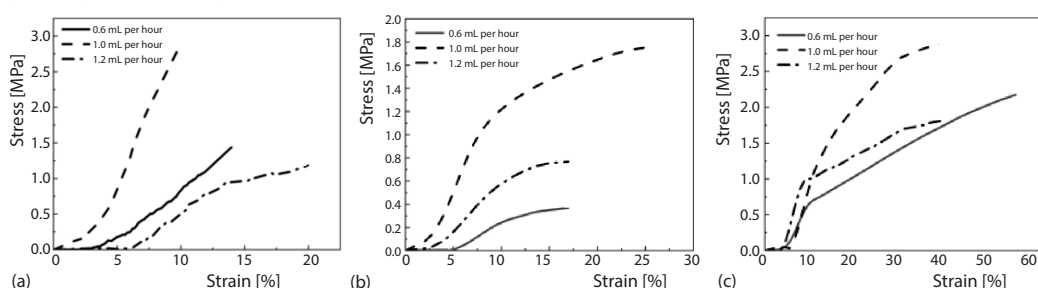


Figure 4. The stress-strain curves of PAN nanofibrous membranes fabricated under certain concentration; (a), (b), and (c) show the stress-strain curves of PAN nanofibrous membranes at the solution concentrations of 8%, 10%, and 12%, respectively

Figure 4 describes the stress-strain curves of nanofibrous membranes under different processing parameters. From fig. 4, it can be clearly observed that at the same solution concentration, the breaking strength first increases and then decreases as the flow rate increases. When the solution concentration increases to 12%, the breaking strength and breaking elongation reach maxima of 56.80% (at the flow rate of 0.6 mL/h) and 3.05 MPa (at the flow rate of 1.0 mL/h), separately. In addition, it can be seen that the breaking strength is weakened from fig. 4(a) and the breaking elongation is somewhat improved fig. 4(b). By comparing 8% and 12% of the fiber membranes, it can be found that the breaking strength are almost the same at the same flow rates, but there is a significant improvement in breaking elongation, nearly twice that.

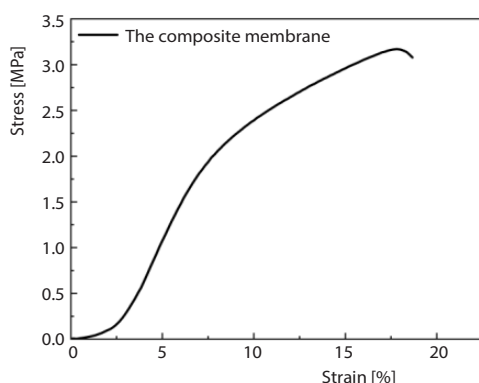


Figure 5. The stress-strain curve of the PAN composite membrane with the solution concentrations of 8%, 10%, and 12% (applied voltage: 18 kV, flow rate: 1.0 mL/h)

Finally, in this part, we also compared the mechanical properties of monolayer and composite membranes. Figure 5 shows the stress-strain curve of the composite membrane. The specific values are listed in tab. 2. It was found that the breaking strength of the composite membrane was improved greatly in comparison with those of monolayer membranes. In addition, the breaking elongation of the composite membrane was only improved in comparison with that of 8% monolayer membrane. On one hand, PAN nanofiber membranes have good mechanical properties, and the breaking strength of monolayer membranes ranged from 1.7 -3.1 MPa. On the other hand, nanofibers of different scales are compounded by layer-by-layer

er to fabricate the composite membranes. When the nanofibers with different diameters come into contact, the number of fiber contact points and the cohesive force increases, so the mechanical properties are improved.

Table 2. The breaking strength and elongation of monolayer membranes and composite membranes

Monolayer/composite membranes	Flow rate [mLh ⁻¹]	Breaking strength [MPa]	Breaking elongation [%]
8 % monolayer	1.0	2.63 ± 0.11	9.08 ± 3.39
10 % monolayer		1.77 ± 0.25	24.33 ± 2.16
12 % monolayer		3.05 ± 0.22	39.46 ± 5.56
Composite membrane		3.17 ± 0.38	17.84 ± 2.21

Figure 6 exhibits the pore size distribution of PAN composite membranes. The porosity P was calculated by the following eq. (1), and the results are shown in tab. 3. It can be seen from fig. 6 and tab. 3 that the PAN composite membrane has a small pore size and a uniform distribution. The average pore diameter of 1.51 μm and the porosity of 91% were obtained separately. Based on these data, the composite membranes were expected to be able to effectively block PM2.5 and had good air permeability in the field of protection:

$$P = \frac{\frac{M}{\rho}}{\frac{M}{\rho} + \frac{M_m}{\rho_m}} \times 100\% \quad (1)$$

where M [g] is the mass of n -butanol absorbed by electrospinning, M_m [g] – the quality after electrospinning, ρ [gcm⁻³] – the n -butanol density, ρ_m [gcm⁻³] – the density of polymer material.

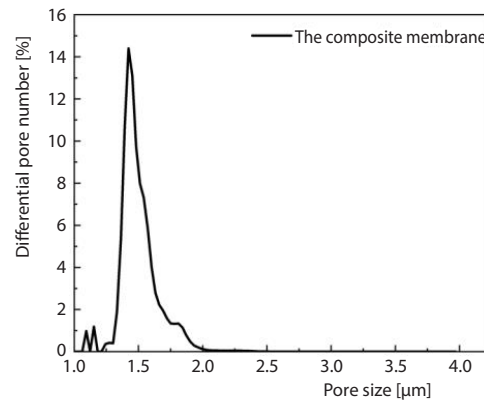


Figure 6. The pore size distribution of PAN composite membranes

Table 3. Pore size distribution and porosity of PAN composite membrane

Sample	Average pore size [μm]	Pore density [cm ⁻²]	Porosity [%]
Composite membrane	1.51	1.3 × 10 ⁷	91

Filtration properties of fiber membranes

The filtration properties of fiber membrane is listed in tab. 4. From tab. 4, the filtration efficiency of PAN composite membranes was up to 99.992%, which was higher than those of the monolayer membranes. The larger the fiber diameter, the worse the filtration performance. In addition, it can be seen that the composite membrane has the best filtration properties with the thickness of 20 μm. The composite membrane can better filter air and aerosols due to its hierarchical structure. This was achieved by electrospinning, which makes the voids among the fibers change stepwise.

Table 4. Comparison of filtration properties of monolayer and composite membranes

Monolayer/composite membranes	Flow rate [mLh ⁻¹]	Thickness [μm]	Transmission rate [%]	Filtration efficiency [%]
8% monolayer	1.0	19	0.017	99.983
10% monolayer	1.0	28	0.019	99.981
12% monolayer	1.0	17	0.026	99.974
Composite membrane	1.0	20	0.008	99.992

Conclusion

In this work, the PAN monolayer/composite nanofibrous membranes were successfully fabricated. The results showed that the influence of flow rate on fiber diameter was considered to be more significant than that of solution concentration. In addition, the breaking strength of the composite membrane was improved greatly in comparison with those of monolayer membranes. The composite membranes with a high porosity showed a better aerosol filtration performance than that of the monolayer membranes. In summary, there is no doubt that this new composite method also provides a novel idea for the design of filter material and the field of air pollution protection.

Acknowledgment

The work is supported by Nantong Science and Technology Project under Grant No. JC2019009 and Technology Guiding Project of China National Textile and Apparel Council under Grant No. 2019010 and Priority Academic Program Development of Jiangsu Higher Education Institutions (PAPD).

References

- [1] Horton, D. E., *et al.*, Occurrence and Persistence of Future Atmospheric Stagnation Events, *Clim. Change*, 4 (2014), 8, pp. 698-703
- [2] Li, H. C., *et al.*, Particulate Matter Exposure and Stress Hormone Levels, *Circulation*, 136 (2017), 7, pp. 618-649
- [3] Hoek, G., *et al.*, Long-Term Air Pollution Exposure and Cardio-Respiratory Mortality: A Review, *Environ. Health*, 12 (2013), May, 43
- [4] Zhang, R. F., *et al.*, Nanofiber Air Filters with High-Temperature Stability for Efficient PM_{2.5} Removal from the Pollution Sources, *Nano Letters*, 16 (2016), 6, pp. 3642-3649
- [5] Zhang, Y. Y., *et al.*, Preparation of Nanofibrous Metal-Organic Framework Filters for Efficient Air Pollution Control, *Journal Am. Chem. Soc.*, 138 (2016), 18, pp. 5785-5788
- [6] Zhang, B. A., *et al.*, Recent Advances in Electrospun Carbon Nanofibers and Their Application in Electrochemical Energy Storage, *Prog. Mater. Sci.*, 76 (2016), Mar., pp. 319-380
- [7] Matulevicius, J., *et al.*, The Comparative Study of Aerosol Filtration by Electrospun Polyamide, Polyvinylacetate, Polyacrylonitrile and Cellulose Acetate Nanofiber Media, *Journal Aerosol Sci.*, 92 (2016), Feb., pp. 27-37
- [8] Lv, D., *et al.*, Ecofriendly Electrospun Membranes Loaded with Visible-Light Responding Nanoparticles for Multifunctional Usages: Highly Efficient Air Filtration, Dye Scavenging, and Bactericidal Activity, *ACS Appl. Mater. Interfaces*, 11 (2019), 13, pp. 12880-12889
- [9] Huang, X. X., *et al.*, Hierarchical Electrospun Nanofibers Treated by Solvent Vapor Annealing as Air Filtration Mat for High Efficiency PM_{2.5} Capture, *Sci. China Mater.*, 62 (2019), 3, pp. 423-436
- [10] Al-Attabi, R., *et al.*, High Efficiency Poly(acrylonitrile) Electrospun Nanofiber Membranes for Airborne Nanomaterials Filtration, *Adv. Eng. Mater.*, 20 (2018), 1, 1700572
- [11] Al-Attabi, R., *et al.*, Pore Engineering Towards Highly Efficient Electrospun Nanofibrous Membranes for Aerosol Particle Removal, *Sci. Total Environ.*, 625 (2018), Jan., pp. 706-715

- [12] Canalli, B. A. C., Composites Based on Nanoparticle and PAN Electrospun Nanofiber Membranes for Air Filtration and Bacterial Removal, *Nanomaterials*, 9 (2019), 12, pp. 1739-1742
- [13] Chen, K. N., et al., Multifunctional TiO₂/Polyacrylonitrile Nanofibers for High Efficiency PM2.5 Capture, UV Filter, and Anti-Bacteria Activity, *Appl. Surf. Sci.*, 493 (2019), Nov., pp. 157-164
- [14] Yin, J., et al., Numerical Approach to High-throughput of Nanofibers by a Modified Bubble-Electrospinning, *Thermal Science*, 24 (2020), 4, pp. 2367-2375
- [15] Ahmed, A., Xu, L., Numerical Analysis of the Electrospinning Process for Fabrication of Composite Fibers, *Thermal Science*, 24 (2020), 4, pp. 2377-2388
- [16] Li, X. X., et al., Nanofibers Membrane for Detecting Heavy Metal Ions, *Thermal Science*, 24 (2020), 4, pp. 2463-2468
- [17] Li, X. X., et al., The Effect of Sonic Vibration on Electrospun Fiber Mats, *Journal of Low Frequency Noise Vibration and Active Control*, 38 (2019), 3-4, pp. 1246-1251
- [18] Zhao, J. H., et al., Needle's Vibration in Needle-Disk Electrospinning Process: Theoretical Model and Experimental Verification, *Journal of Low Frequency Noise Vibration and Active Control*, 38 (2019), 3-4, pp. 1338-1344
- [19] Wu, Y. K., Liu, Y., Fractal-Like Multiple Jets in Electrospinning Process, *Thermal Science*, 24 (2020), 4, pp. 2499-2505
- [20] He, J. H., Advances in Bubble Electrospinning, Recent Patents on Nanotechnology, 13 (2019), 3, pp. 162 -163
- [21] Yao, X., He, J. H., On Fabrication of Nanoscale Non-Smooth Fibers with High Geometric Potential and Nanoparticle's Non-Linear Vibration, *Thermal Science*, 24 (2020), 4, pp. 2491-2497
- [22] Yang, Z. P., et al., A Fractal Model for Pressure Drop through a Cigarette Filter, *Thermal Science*, 24 (2020), 4, pp. 2653-2659
- [23] Li, X. X., He, J. H., Nanoscale Adhesion and Attachment Oscillation under the Geometric Potential – Part 1: The Formation Mechanism of Nanofiber Membrane in the Electrospinning, *Results in Physics*, 12 (2019), Mar., pp. 1405-1410
- [24] He, J. H., Liu, Y. P., Bubble Electrospinning: Patents, Promises and Challenges, *Recent Patents on Nanotechnology*, 14 (2020), 1, pp. 3-4
- [25] He, C. H., et al., Taylor Series Solution for Fractal Bratu-Type Equation Arising in Electrospinning Process, *Fractals*, 28 (2020), 1, 2050011
- [26] He, J. H., On the Height of Taylor Cone in Electrospinning, *Results in Physics*, 17 (2020), June, 103096